Graphene

International Edition: DOI: 10.1002/anie.201706437
German Edition: DOI: 10.1002/ange.201706437

Highly Regioselective Alkylation of Hexabenzocoronenes: Fundamental Insights into the Covalent Chemistry of Graphene

Johannes Holzwarth, Konstantin Yu. Amsharov, Dmitry I. Sharapa, David Reger, Kateryna Roshchyna, Dominik Lungerich, Norbert Jux, Frank Hauke, Timothy Clark, and Andreas Hirsch**

Abstract: *Hexa-peri-hexabenzocoronides (HBC) was successfully used as a model system for investigating the complex mechanism of the reductive functionalization of graphene. The well-defined molecular HBC system enabled deeper insights into the mechanism of the alkylation of reductively activated nanographenes. The separation and complete characterization of alkylation products clearly demonstrate that nanographene functionalization proceeds with exceptionally high regio- and stereoselectivities on the HBC scaffold. Experimental and theoretical studies lead to the conclusion that the intact basal graphene plane is chemically inert and addend binding can only take place at either preexisting defects or close to the periphery.*

The chemistry of two-dimensional (2D) materials is currently an emerging field located at the interface between chemistry, physics, and materials science. The archetype of such planar architectures is graphene,[1] a single sheet of graphite, which represents a hexagonal network of sp^2-configured carbon atoms. Covalent functionalization[2–8] of graphene allows the combination of its unique properties[9,10] with those of other classes of compounds. The chemical consequence of the covalent addend binding is the rehybridization of the carbon atom, to which the addend is bound, from its initial sp^2 to an sp^3 configuration. This process can also be considered as an introduction of basal plane defects which lead to the modification of the electronic (band structure), optical, and mechanical properties. In contrast, the covalent addition chemistry offers the opportunity to improve the solubility and processability, thus facilitating the manufacturing processes required for practical applications. Another highly appealing aspect of covalent graphene functionalization is the desire to discover fundamental reactivity principles within the largely unexplored realm of 2D chemistry. The most efficient method for covalent graphene functionalization is the treatment of negatively charged graphenide sheets with electrophiles, a method we introduced a few years ago,[11] and which since then, has been continuously improved.[12–21] This reductive approach allows the generation of a large variety of covalent adducts, including alkylated, arylated, and hydrogenated graphene derivatives, which exhibit comparatively high degrees of addition. Together with the reductive bulk functionalization, the addition chemistry of graphenides deposited on surfaces[18–21] has been investigated. The key point is the use of negatively charged graphites, the so called graphite intercalation compounds (GICs), as starting materials. In GICs, alkaline metals, such as potassium, are placed between the individual carbon sheets and the graphene layers are reductively activated by electron transfer from the metal intercalates. A general feature of reductive graphene functionalization protocols seems to be an inhomogeneous distribution of addends on the surface and leads to the formation of islands of highly functionalized areas next to intact nanographenes. This distribution has been demonstrated, for example, by high-resolution transmission-electron microscopy (HRTEM) of polyarylated graphene,[11] and fluorescence spectroscopy of hydrogenated graphene.[13] Despite these first successful developments, many questions concerning the reaction mechanism, including the precise sequence of activation, electron transfer, and propagation steps as well as the regiochemisty of the covalent addend binding, the role of pre-existing defects, both within the basal carbon plane and at the edges, the inertness or reactivity of the intact basal plane, and the exact nature of the electrophile (e.g. steric demand, redox potential) remained unanswered. One reason for this lack of knowledge is the difficulty in precise and unambiguous characterization of the reaction products, as the common powerful tools for the structure elucidation of molecules, such as NMR spectroscopy and mass spectrometry, cannot be used for these polydisperse carbon allotropes. Instead, indirect methods such as TEM, scanning Raman microscopy (SRM),[14,18] and thermogravimetric analysis (TGA) coupled

[*] Dr. J. Holzwarth, Dr. F. Hauke, Prof. A. Hirsch
Joint Institute of Advanced Materials and Processes (ZMP), Friedrich-Alexander University of Erlangen-Nürnberg
Dr. Mack-Str. 81, 90762 Fürth (Germany)
Dr. K. Y. Amsharov, D. Reger, Dr. K. Roshchyna, Dr. D. Lungerich, Prof. N. Jux, Prof. A. Hirsch
Department of Chemistry and Pharmacy & Interdisciplinary Center for Molecular Materials
Friedrich-Alexander University of Erlangen-Nürnberg,91054 Erlangen (Germany)
E-mail: konstantin.amsharov@fau.de
andreas.hirsch@fau.de
Dr. D. I. Sharapa, Prof. T. Clark
Computer-Chemie-Centrum, Friedrich-Alexander University of Erlangen-Nürnberg
Nägelsbachstraße 25, 91058 Erlangen (Germany)
Supporting information and the ORCID identification number(s) for the author(s) of this article can be found under: https://doi.org/10.1002/anie.201706437.

with gas chromatography and mass spectrometry[15] had to be adapted and applied for their structural characterization. It is also important to point out that functionalized graphene samples represent polydisperse macrcomolecules, which impede experimental and computational investigations further. One approach to address this challenge would be the careful simulation of reductive graphene functionalization, using small model compounds, with a defined and monodisperse structure. In this case, separation of reaction products, precise structural characterization, and simulation of the entire reaction energetics using high-level quantum mechanical calculations would be possible.

Our current study sets out to provide fundamental insights into the reductive functionalization of 2D nanocarbons. As a molecular model, we chose the hexa-*peri*-hexabenzocoronene (HBC) platform, which represents a substructure of the graphene sheet with a graphene-like π surface (Figure 1).[22–29]

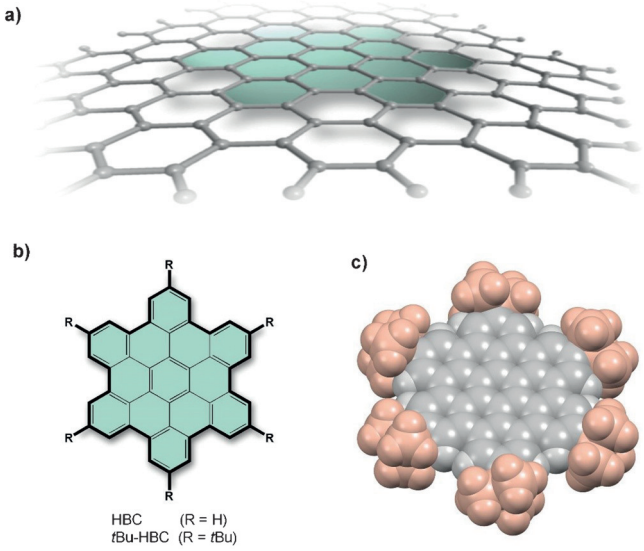

Figure 1. a) Hexa-*peri*-hexabenzocoronene, a small structural element of a graphene section. The HBC fragment is highlighted in green. b) HBC and *t*Bu-HBC used in this work as a graphene model. c) Space-filling model of *t*Bu-HBC showing an effective protection of the nanographene periphery. Bulky *t*Bu groups are highlighted in brown. The graphene-like surface is shown in grey.

Prior to the reaction with alkyl iodides, HBC was activated by transformation to the dianion (HBC^{2-}). We have also used hexa-*tert*-butylated HBC (*t*Bu-HBC) as the starting material, in which the *tert*-butyl groups provide enhanced solubility and shielding of the periphery (Figure 1c). We were able to isolate and characterize the respective bis(alkyl)ated adducts in detail. Significantly, the reaction proceeded highly regioselectively, since only two regioisomers with a peripheral *anti*-1,2- and *anti*-1,4 addition pattern were formed as major products. Guided by density-functional theory (DFT) calculations, we were able to reveal fundamental mechanistic insights of the entire addition process, which provides the desired guidelines for understanding the 2D chemistry of graphene.

As well-defined molecular graphene models HBC and *t*Bu-HBC (Figure 1b), which feature both graphene-like edges and an extended π surface, were chosen. Whereas in HBC the ratio of accessible edge versus in-plane carbon atoms is rather high, the steric demand of the *tert*-butyl groups is expected to shield the edges effectively, thus forcing the chemistry to take place predominantly on the graphene-like π surface. Importantly the HBC π system is characterized by the highest possible numbers of Clar sextets arranged in a D_{6h}-symmetrical manner. The corresponding pronounced benzenoid character is reminiscent of that of graphene.[30] To achieve a high comparability, the same reaction conditions as those previously used for the corresponding reductive graphene chemistry were chosen. Here, activated graphite in the form of alkali metal intercalation compounds (GICs) was used as starting material.[11,12] Alkyl iodides (Table 1) were

Table 1: Overview of the applied electrophiles with corresponding yields for both isomers.

R	Electrophile	Yield [%] 1,4 adduct 2,3′-(*t*Bu-HBC)R_2	1,2 adduct 2,3-(*t*Bu-HBC)R_2
Me		< 3	54
Et		9	48
Hex	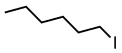	17	24
*i*Pr		42	9
*t*Bu		< 5	–

tested as organic trapping electrophiles, thus allowing the elucidation of the structure–reactivity relationships and providing further insight into the mechanism of the addition. The synthesis of the salts K_2[HBC] and K_2[*t*Bu-HBC] was carried out by melting two equivalents of potassium with the respective hexabenzocoronene at 570 K for 48 hours. This reductive salt formation was indicated to be complete by a color change from bright yellow to dark red-brown. The oxygen- and moisture-sensitive salts K_2[HBC] and K_2[*t*Bu-HBC] were characterized by absorption spectroscopy under inert conditions and showed the typical bathochromic shift of the narrow and intense absorption band of pristine HBC at $\lambda = 360$ nm to a broad absorption in the near infrared.[31] In analogy to either the wet chemical alkylation or arylation of GICs, the salts K_2[HBC] and K_2[*t*Bu-HBC] were dissolved in a small amount of absolute THF under inert conditions, and resulted in the formation of dark red solutions. On slow addition of a tenfold excess of the alkyl iodide under an argon atmosphere, the solution first turned green and finally to orange while developing an increasing fluorescence. After multistep HPLC separation, all major components of the reaction mixtures were analyzed by high-resolution mass spectrometry (HRMS) and NMR spectroscopy. Interestingly, quenching of K_2[*t*Bu-HBC] with MeOH was accompanied by the recovery of *t*Bu-HBC without any sign of hydrogenation

of the HBC core. HPLC-MS analysis of the alkylated *t*Bu-HBC reveals that in most cases the major components of the crude reaction mixture are the expected bis(adduct)s (*t*Bu-HBC)R_2 formed together with reoxidized *t*Bu-HBC. Interestingly, small amounts of tetrakis and hexakis adducts, (*t*Bu-HBC)R_4 and (*t*Bu-HBC)R_6, respectively, were also formed (Figure 2). Remarkably, careful NMR analysis of the bis(adduct)s (*t*Bu-HBC)R_2 revealed that only two of 136 possible isomers were formed. The addition pattern was elucidated unambiguously by means of 2D NMR techniques, including COSY, DEPT-Q, HSQC, and HMBC (for details see the Supporting Information). The reaction sequence yielding the isolated major products is outlined in Figure 2a.

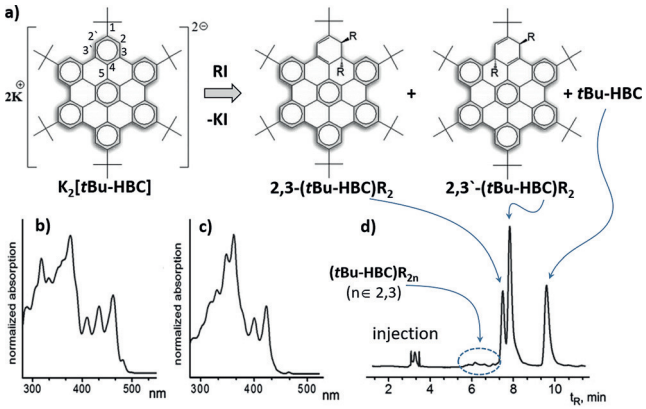

Figure 2. a) Reductive alkylation of K_2[*t*Bu-HBC] with a variety of alkyl iodides (see Table 1) and the main isolated products. The numbering of the different carbon positions is shown for K_2[*t*Bu-HBC]. The reaction products 2,3-(*t*Bu-HBC)R_2 and 2,3′-(*t*Bu-HBC)R_2 were formed by an *anti*-1,2- and *anti*-1,4-addition reaction, respectively. Typical UV/Vis spectra of 2,3-(*t*Bu-HBC)R_2 (b) and 2,3′-(*t*Bu-HBC)R_2 (R = ethyl; c) are shown. The bathochromic shift of *anti*-2,3-(*t*Bu-HBC)R_2 is due to the contribution of two localized double bonds to the conjugated π system, which is in contrast to the *anti*-2,3′-(*t*Bu-HBC)R_2 situation, containing only one conjugated double bond. The nature of the alkyl group R has only little influence on the UV/Vis spectra (see the Supporting Information). d) Typical HPLC profile of the crude reaction mixture after alkylation, detected at $\lambda = 350$ nm (shown for the ethylation).

Analogous to the functionalization of the C_{60} dianion (C_{60}^{2-}),[32] it turned out that the two isolated isomers involve either a 1,2- or a 1,4-addition pattern. However, in contrast to the spherical C_{60} fullerene, which can only undergo supratopic exohedral *syn* additions, the HBC scaffold also allows antratopic *anti* additions, so that a priori a large variety of different *syn* and *anti* regioisomers is conceivable. The same arguments also hold for dispersed graphene. NOESY experiments (for details, see the Supporting Information), carried out to investigate the stereochemistry of the addition, showed that exclusively *anti* additions took place. To corroborate these findings, K_2[*t*Bu-HBC] was reacted with bifunctional 1,6-diiodohexane. The concentration of diiodohexane was kept very low by slow addition of the diluted alkyl iodide solution to the *t*Bu-HBC dianion. Despite favorable conditions for an intramolecular cycloaddition, no *syn* adducts were detected in the reaction mixture. Instead, the formation of a twofold iodohexylation was observed. This result also demonstrates the very pronounced preference of *anti* additions to the nanographene sheet (for details see the Supporting Information).

Of all the aliphatic iodides tested, the 1,2- and 1,4-*anti*-adducts **2**,**3**-(*t*Bu-HBC)R_2 and **2**,**3**′-(*t*Bu-HBC)R_2 were exclusively yielded. Table 1 summarizes the results for the different aliphatic iodides used over the course of the reductive alkylation of K_2[*t*Bu-HBC] and the corresponding yields of for both isolated isomers. One fundamental finding is that the isomeric ratio is strongly influenced by the steric demand of the alkyl iodide. For hexyl iodide, the ratio between the 1,2- and 1,4-adduct was found to be close to 1:1, whereas the reaction with ethyl iodide led to a product distribution in which the corresponding 1,2-adduct is favored. On decreasing the alkyl chain length further by using methyl iodide, the reaction afforded almost exclusively the 1,2-adduct. In contrast, treatment with isopropyl iodide resulted mainly in the 1,4-adduct. To increase the steric demand of the electrophile further, *tert*-butyl iodide was tested. In this case, the reaction proceeded very slowly and led mainly to reoxidized pristine *t*Bu-HBC. Nevertheless, very small amounts of 1,4-adducts, but no formation of the 1,2-adduct, were detected in this case. As a reference, the dianion of the unsubstituted HBC was functionalized analogously with hexyl iodide. Significantly, although in this case positions 1 and 2 are not sterically shielded, virtually the same regioselectivity was observed, thus leading to the same major products with the *anti*-1,2- and 1,4-addition patterns, namely, 2,3-(HBC)R_2 and 2,3′-(HBC)R_2. Although the formation of polyalkylated derivatives of HBC is more pronounced than in the *t*Bu-HBC system (see the Supporting Information), this finding clearly demonstrates that the steric shielding of the periphery is not relevant for the product distribution. Note that the tentatively expected formation of 1,2-(HBC)R_2 was not observed. The most significant finding of these addition studies is that the graphene-like π plane itself, and not the nature of the edge substituents, largely dictates the specific reactivity pattern, which in turn directs the addends to the periphery. The periphery, in contrast, can be considered as cuts or defects in the π plane. This behavior is in stark contrast to the widely accepted assumption that the periphery of graphene is more reactive than the inner π surface. The observed high regio- and stereoselectivity of the HBC alkylation as such is also very remarkable. Although the driving force for 1,2- and 1,4-additions can be explained by retaining the maximum number of isolated Clar sextets (both isomers have six intact benzene-like substructures (Figure 2a), the formation of only these two major isomers cannot be rationalized by Clar's rule alone. For instance, the absence of 1,2-(HBC)R_2, which exhibits the same number of Clar sextets, is unexpected. To provide further insight into the high regio- and stereoselectivity, we carried out a series of systematic quantum chemical calculations. Based on DFT calculations, a three-step mechanism of the reductive nanographene alkylation can be supported (Figure 3). Note, for both *t*Bu-HBC and H-terminated HBC, the stability of regioisomers and the energetics of transition states were found to be qualitatively the same, unless specially specified. The first step in the reaction sequence is the

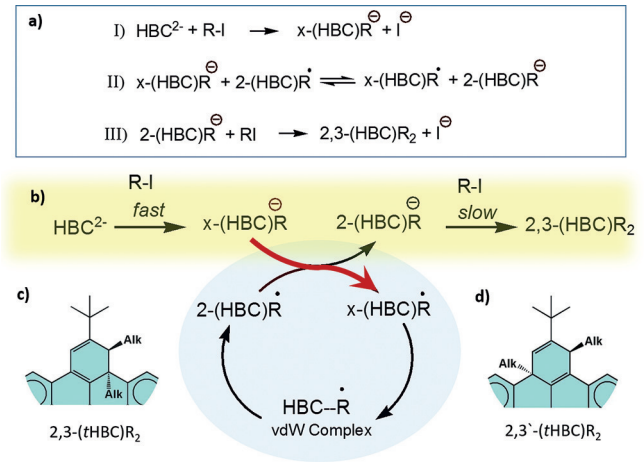

Figure 3. a, b) General three step mechanism of the reductive alkylation of HBCs with alkyliodides. The main pathway is highlighted in yellow. c) Key radical cycle is highlighted within the blue frame. 2-(HBC)R denotes the HBC core alkylated in position 2. *x*-(HBC)R corresponds to the random attachment ($x \in 1,2,3,4,5$). c,d) Structural fragments of experimentally observed *t*Bu-HBC bis(adduct)s.

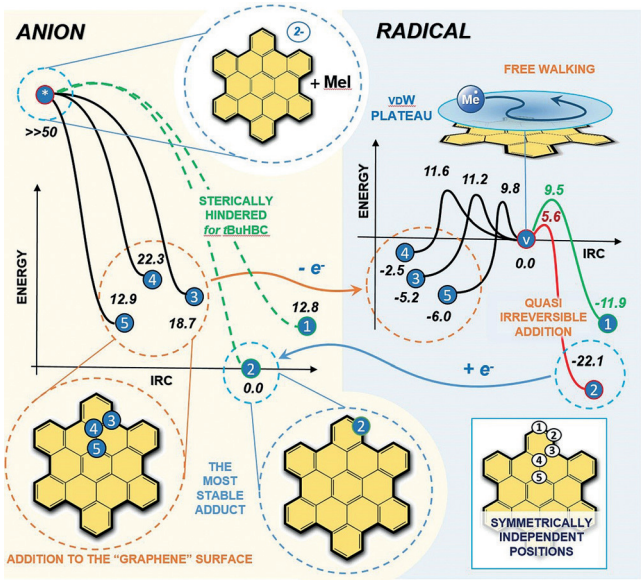

Figure 4. Detailed mechanism of the first and second steps of the reductive HBC alkylation with methyl iodide. Numbers within blue circles indicate the carbon position on the HBC scaffold. The asterisk (*) denotes the starting point. In the case of the alkylation of *t*Bu-HBC, the pathways indicated by dashed green lines are sterically hindered. The numbers in circles correspond to the carbon atom positions according to the numbering given in inset. All energies are given in kcal mol^{-1} for the H-terminated HBC.

previously suggested single-electron transfer (SET),[17] from the corresponding HBC dianion to the alkyl halide, accompanied by an alkylation and I^- release, thus leading to a regioisomeric mixture of monoalkylated anions $(HBC\text{-}R)^-$ (first step). This step is coupled to a redox-equilibrium between monoanions $(HBC\text{-}R)^-$ and the oxidized radicals $(HBC\text{-}R)^\bullet$. The formation of the latter species can be provided by an additional oxidation with intact alkyl iodide, which was applied in a tenfold excess. As will be pointed out below, very facile movement of $R^\bullet$ between the 2–5 positions is possible within the radicals $(HBC\text{-}R)^\bullet$, thus allowing easy formation of the thermodynamically most favorable isomer of $(HBC\text{-}R)^-$, in which the position of the addend R is locked after subsequent reduction. The last step in the formation of $HBC\text{-}R_2$ is a kinetically controlled stereoselective S_N2-like alkylation, which will be discussed below.

The proposed reaction mechanism, which is supported by both experimental findings and the quantum mechanical calculation, is discussed in more detail. The first step in the reaction between the HBC-dianion and alkyl iodide is a SET from the HBC dianion to the alkyl iodide. This fast process has been reported in the chemistry of fullerenes,[32] carbon nanotubes,[33–38] and particularly for the reductive alkylation and arylation of graphene.[15,21] The SET is a very fast process which leads to the anion radical of the corresponding alkyl iodide and subsequently releases an iodide, while the simultaneously formed alkyl radical $R^\bullet$ attacks a carbon atom of the HBC anion radical just generated. DFT calculations of the corresponding reaction coordinate show that this process is highly exergonic and has virtually no activation barrier. This first step is essentially irreversible as the activation barrier for the back-reaction is very high (> 50 kcal mol^{-1}). A priori, a mixture of five possible regioisomers of the anionic adducts $(HBC\text{-}R)^-$ is possible. In the case of *t*Bu-HBC, however, an attack on the sterically hindered positions 1 and 2, on the edges, is strongly suppressed, while the addition to the quaternary positions 3, 4, and 5 remains favorable (Figure 4). The resulting anions could, in principle, react directly with another molecule of alkyl iodide by an S_N2/SET mechanism, thus leading to the depicted bis(adduct)s. However, a large number of possible regioisomers would be formed within such a scenario, and is in contrast to the experimental observations. In contrast, our DFT calculations show that a facile migration of the first alkyl addend to the thermodynamically favorable position 2 is impossible for the monoanions $HBC\text{-}R^-$, but possible for the radicals $(HBC\text{-}R)^\bullet$. It is reasonable to assume a redox equilibrium between $(HBC\text{-}R)^-$ and $(HBC\text{-}R)^\bullet$ with a high mobility of R on the π surface of the HBC. This mobility allows the formation of the thermodynamically most stable anion $(HBC\text{-}R)^-$ with R bound at position 2. Importantly, this entire cyclic sequence of oxidation, migration, and reduction (Figure 3c), which leads to the thermodynamically most stable isomer 2-$(HBC\text{-}R)^-$, and can be considered as hole-catalysis.[39] Small amounts of monoalkylated HBC radicals can be formed directly by the reaction between the anion $(HBC\text{-}R)^-$ and alkyl iodide, which is used in a tenfold excess. Alternative electron-exchange processes between charged educts, intermediates, and neutral products could also be operative. Independent of the electron-hole source, the coupled equilibria between $(HBC\text{-}R)^-$ and $(HBC\text{-}R)^\bullet$ will always lead to the regioselective formation of 2-$(HBC\text{-}R)^-$. The presence of redox equilibria between neutral, mono-, and dianionic HBC derivatives with different degrees of addend binding nicely explains the formation of tetrakis and hexakis adducts such as $(t\text{Bu-HBC})R_4$ and $(t\text{Bu-HBC})R_6$, respectively, formed in small quantities as side products (Figure 2).

Our calculations show that (HBC-R)$^{\bullet}$ with alkyl groups attached to positions 1, 3, 4, and 5 can reversibly form van der Waals (vdW) complexes at room temperature. Such a non-covalent binding of radicals has been predicted theoretically for the graphene surface.[20] However, unexpectedly, this process also appears to be feasible for the peripheral carbon atom in position 1 in unprotected HBC. The barriers of these transformations were found to be as low as 14–21 kcal mol^{-1} (and 10–11 kcal mol^{-1} for the back reaction) in the case of methyl radicals. These barriers become even lower with increasing stability of the alkyl radical (see the Supporting Information). Practically free migration of R on the π surface of the HBC is possible in such vdW complexes of alkyl radicals. The corresponding vdW energy hypersurface contains neither well-defined minima nor unstable regions, and covers the whole nanographene surface up to the edges (edges are not included, for details see the Supporting Information). At the same time, the barrier to covalent attachment in position 2 was found to be 5 kcal mol^{-1} lower and the resulting regioisomer 2-(HBC-R)$^{\bullet}$ represents a thermodynamic minimum with a relatively high barrier for the back-reaction to the vdW complex (27.6 kcal mol^{-1}). After formation of 2-(HBC-R)$^{-}$, the final nucleophilic substitutions to 2,3-(HBC)R_2 and 2,3′-(HBC)R_2 can take place (Figure 3c). Our calculations show that the direct alkylation of monoalkylated (HBC-R)$^{\bullet}$ by RI is highly unlikely because of its high activation barrier. However, the monoalkylated vdW complex HBC-R$^{\bullet}$ can eliminate an alkylradical R$^{\bullet}$ rather easily, thus leading to the recovery of the initial HBC. The corresponding dissociation energy was calculated to be 5–10 kcal mol^{-1}, depending on the nature of R (see the Supporting Information). Indeed, we find neutral HBC to be the main by-product.

In contrast to the initial alkylation, the covalent binding of the second alkyl group is kinetically controlled. The most important difference is that (HBC-R)$^{-}$ is a much weaker reductant than HBC^{2-}, and disfavors the corresponding SET to the alkyl iodide. As can be seen from Figure 5a, in 2-(HBC-R)$^{-}$ the coefficients of the HOMO are mainly localized on the positions 3 and 3′. The corresponding carbon atoms are suitable nucleophilic centers for a S_N2-like alkylation. In contrast, the HOMO of the dianion HBC^{2-} is delocalized over the whole π surface (see the Supporting Information). Consequently, the alkylation of (HBC-R)$^{-}$ leading to HBC-R_2 can occur by an S_N2-like mechanism (S_N2-mechanism with coupled SET[40]). The product distribution between the 1,2- and 1,4-adducts listed in Table 1 strongly supports the S_N2 character of the second addition step. The DFT calculations also show that *syn* additions are characterized by significantly higher activation barriers than the more favorable *anti* additions (see also the Supporting Information). Note that the SET character of S_N2 process is considered by DFT calculations. The barriers for *syn* additions were always found to be more than 2.2 kcal mol^{-1} (typically over 5 kcal mol^{-1}) higher. This finding suggests that less than 2% of the competing *syn* additions should be observed. The regioselectivity of *anti* addition is mainly controlled by the steric requirement of the alkyl substituents. In the case of the methyl group, the activation barrier for *syn* binding into position 3 is 2.5 kcal mol^{-1} higher than the respective *anti* attachment to same position. Corroborating our experimental findings, this leads to the preferred formation of *anti*-2,3-(HBC)Me_2. However, in going from Me to Et and *i*Pr, the energy differences of the activation barriers decrease to less than 0.5 kcal mol^{-1}, thus reaching the limits of accuracy of the DFT calculations applied and, as a consequence, both isomers *anti*-2,3-(HBC)R_2 and *anti*-2,3′-(HBC)R_2 should be expected in the product mixture. These results are in excellent agreement with our experimental data (see Table 1). A very characteristic feature of the second alkylation step is that it always occurs in close proximity to the position of the first addend binding and displays a high preference for *anti* additions. The fact that the reaction with *tert*-butyl iodide yields only very small amounts of bis(adduct)s corroborates the postulated S_N2-character of the final alkylation step. Interestingly, the DFT calculations predict the same regioselectivity for alkylation of both partially shielded *t*Bu-HBC and H-terminated HBC. This regioselectivity clearly reflects the weak influence of the nature of the periphery on the mode of functionalization. Indeed, the alkylation of unprotected HBC leads exclusively to the same 2,3- and 2,3′-(HBC)R_2 isomers. Moreover, the absence of the 1,2-(HBC)R_2 isomer is in excellent agreement with the proposed mechanism.

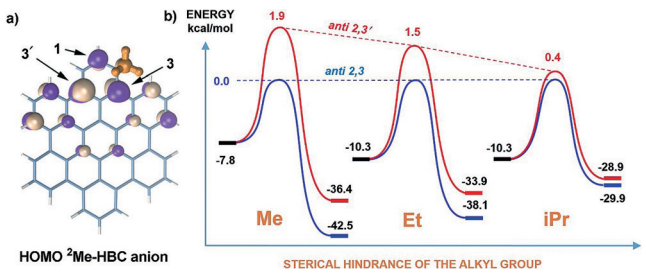

Figure 5. a) Pronounced HOMO coefficients of (2-HBC-Me)$^{-}$ in positions 3 and 3′. b) Schematic representation of the intrinsic reaction pathways for the final S_N2-like alkylation.

Summing up, we have successfully employed hexa-*peri*-hexabenzocoronides as a model system for investigating the complex mechanism of the reductive functionalization of graphene. The well-defined molecular HBC system enabled us to gain deeper insights into the mechanism of the alkylation of reductively activated nanographenes. The separation and complete characterization of the alkylation products clearly demonstrates that nanographene functionalization proceeds with exceptionally high regio- and stereoselectivities on the HBC scaffold. Based on our findings, supported by high-level calculations, we postulate that the first alkylation step takes place on the graphene surface after a preceding SET step, with subsequent migration of the alkyl group to a defect/edge position, where finally irreversible covalent bonding to the nanographene scaffold takes place. As a result, the functional moiety introduced within the initial alkylation step is always observed at the edges (or defect). Similar behavior was previously observed for hydrogenation and chlorination of nanographenes.[41,42]

The second alkylation step takes place in close proximity to the first addend and follows an S_N2-like mechanism. The

free movement of alkyl radicals in the neutral vdW complex HBC-R• is a key step of the entire sequence, and is supported by electron-hole catalysis. Transferring these insights to the extended graphene plane leads to the conclusion that the covalent alkylation of an ideal defect-free graphene surface is highly unlikely. In other words, our findings show that alkylation of reductively activated graphene can only take place at preexisting defects or close to the periphery. Such a scenario ultimately leads to the progressive expansion of functionalized regions around intrinsic defects and the periphery. As already anticipated and based on our previous studies,[11,13] no homogeneous addend binding on the graphene surface can be expected. In general, our results provide the first experimental evidence of the free migration of the trapped radical species over the graphene surface, and arises from the characteristic combination of graphene surface reactivity and the impossibility to form stable covalent adducts far away from defects. This finding opens new avenues in the understanding of the chemistry of graphene and it could potentially extend the scope of possible applications of graphene-based nanomaterials remarkably.

Experimental Section

General procedure of HBC alkylation: 1 equiv of dry HBC (or *t*Bu-HBC) was molten under inert conditions in a glove box together with 2 equiv of distilled elemental potassium. The solids were heated to 300 °C at a pressure of 50 mbar for 72 h. The obtained salt K_2[HBC] (or K_2[*t*Bu-HBC]) was dissolved in absolute THF. The respective alkyl iodide was added slowly in tenfold excess to the corresponding solution. The solvent was removed and the crude reaction mixture was dissolved in toluene, filtered through a microfilter, and subjected to multistep HPLC separation.

Acknowledgements

The authors thank the Deutsche Forschungsgemeinschaft (DFG-SFB 953 "Synthetic Carbon Allotropes", Project A1, A2, A6, C1). The research leading to these results has received partial funding from the European Union Seventh Framework Programme under grant agreement no.604391 Graphene Flagship.

Conflict of interest

The authors declare no conflict of interest.

Keywords: alkylation · density-functional calculations · graphene · radicals · reaction mechanisms

How to cite: *Angew. Chem. Int. Ed.* **2017**, *56*, 12184–12190
Angew. Chem. **2017**, *129*, 12352–12358

[1] K. S. Novoselov, A. K. Geim, S. V. Morozov, D. Jiang, Y. Zhang, S. V. Dubonos, et al., *Science* **2004**, *306*, 666–669.
[2] A. Hirsch, J. M. Englert, F. Hauke, *Acc. Chem. Res.* **2013**, *46*, 87–96.
[3] S. Eigler, A. Hirsch, *Angew. Chem. Int. Ed.* **2014**, *53*, 7720–7738; *Angew. Chem.* **2014**, *126*, 7852–7872.
[4] M. J. Allen, V. C. Tung, R. B. Kaner, *Chem. Rev.* **2010**, *110*, 132–145.
[5] V. Georgakilas, M. Otyepka, A. B. Bourlinos, V. Chandra, N. Kim, K. C. Kemp, et al., *Chem. Rev.* **2012**, *112*, 6156–6214.
[6] S. P. Economopoulos, N. Tagmatarchis, *Chem. Eur. J.* **2013**, *19*, 12930–12936.
[7] Q. Tang, Z. Zhou, Z. Chen, *Nanoscale* **2013**, *5*, 4541–4583.
[8] C. E. Hamilton, J. R. Lomeda, Z. Sun, J. M. Tour, A. R. Barron, *Nano Lett.* **2009**, *9*, 3460–3462.
[9] S. V. Morozov, K. S. Novoselov, M. I. Katsnelson, F. Schedin, D. C. Elias, J. A. Jaszczak, et al., *Phys. Rev. Lett.* **2008**, *100*, 016602.
[10] A. H. Castro Neto, F. Guinea, N. M. R. Peres, K. S. Novoselov, A. K. Geim, *Rev. Mod. Phys.* **2009**, *81*, 109–162.
[11] J. M. Englert, C. Dotzer, G. Yang, M. Schmid, C. Papp, J. M. Gottfried, et al., *Nat. Chem.* **2011**, *3*, 279–286.
[12] K. C. Knirsch, J. M. Englert, C. Dotzer, F. Hauke, F. A. Hirsch, *Chem. Commun.* **2013**, *49*, 10811–10813.
[13] R. A. Schäfer, J. M. Englert, P. Wehrfritz, W. Bauer, F. Hauke, T. Seyller, et al., *Angew. Chem. Int. Ed.* **2013**, *52*, 754–757; *Angew. Chem.* **2013**, *125*, 782–786.
[14] J. M. Englert, P. Vecera, K. C. Knirsch, R. A. Schaefer, F. Hauke, A. Hirsch, *ACS Nano* **2013**, *7*, 5472–5482.
[15] F. Hof, R. A. Schaefer, C. Weiss, F. Hauke, A. Hirsch, *Chem. Eur. J.* **2014**, *20*, 16644–16651.
[16] V. Strauss, R. A. Schaefer, F. Hauke, A. Hirsch, D. M. Guldi, *J. Am. Chem. Soc.* **2015**, *137*, 13079–13086.
[17] R. A. Schäfer, D. Dasler, U. Mundloch, F. Hauke, A. Hirsch, *J. Am. Chem. Soc.* **2016**, *138*, 1647–1652.
[18] K. C. Knirsch, R. A. Schaefer, F. Hauke, A. Hirsch, *Angew. Chem. Int. Ed.* **2016**, *55*, 5861–5864; *Angew. Chem.* **2016**, *128*, 5956–5960.
[19] R. A. Schäfer, K. Weber, M. Kolesnik-Gray, F. Hauke, V. Krstic, B. Meyer, et al., *Angew. Chem. Int. Ed.* **2016**, *55*, 14858–14862; *Angew. Chem.* **2016**, *128*, 15080–15084.
[20] P. Vecera, J. Holzwarth, K. F. Edelthalhammer, U. Mundloch, H. Peterlik, F. Hauke, et al., *Nat. Commun.* **2016**, *7*, 12411.
[21] G. Abellán, M. Schirowski, K. F. Edelthalhammer, M. Fickert, K. Werbach, H. Peterlik, et al., *J. Am. Chem. Soc.* **2017**, *139*, 5175–5182.
[22] X. Feng, J. Wu, V. Enkelmann, K. Muellen, *Org. Lett.* **2006**, *8*, 1145–1148.
[23] R. Liu, D. Wu, X. Feng, K. Mullen, *J. Am. Chem. Soc.* **2011**, *133*, 15221–15223.
[24] F. Cataldo, O. Ursini, G. Angelini, S. Iglesias-Groth, *Fullerenes Nanotubes Carbon Nanostruct.* **2011**, *19*, 713–725.
[25] S. L. Zhang, Z. F. Xue, Y. R. Gao, S. Mao, Y. Q. Wang, *Tetrahedron Lett.* **2012**, *53*, 2436–2439.
[26] P. T. Herwig, V. Enkelmann, O. Schmelz, K. Mullen, *Chem. Eur. J.* **2000**, *6*, 1834–1839.
[27] R. Rathore, C. L. Burns, *J. Org. Chem.* **2003**, *68*, 4071–4074.
[28] S. K. Sadhukhan, C. Viala, A. Gourdon, *Synthesis* **2003**, 1521–1525.
[29] L. Zhai, R. Shukla, R. Rathore, *Org. Lett.* **2009**, *11*, 3474–3477.
[30] J. Wu, W. Pisula, K. Muellen, *Chem. Rev.* **2007**, *107*, 718–747.
[31] A. Fechtenkötter, N. Tchebotareva, M. Watson, K. Muellen, *Tetrahedron* **2001**, *57*, 3769–3783.
[32] S. Fukuzumi, T. Suenobu, T. Hirasaka, R. Arakawa, K. M. Kadish, *J. Am. Chem. Soc.* **1998**, *120*, 9220–9227.
[33] F. Hof, S. Bosch, S. Eigler, F. Hauke, A. Hirsch, *J. Am. Chem. Soc.* **2013**, *135*, 18385–18395.
[34] J. Chattopadhyay, S. Chakraborty, A. Mukherjee, R. Wang, P. S. Engel, W. E. Billups, *J. Phys. Chem. C* **2007**, *111*, 17928–17932.
[35] M. S. Strano, C. A. Dyke, M. L. Usrey, P. W. Barone, M. J. Allen, H. Shan, et al., *Science* **2003**, *301*, 1519–1522.
[36] M. L. Usrey, E. S. Lippmann, M. S. Strano, *J. Am. Chem. Soc.* **2005**, *127*, 16129–16135.

[37] G. Schmidt, S. Gallon, S. Esnouf, J. P. Bourgoin, P. Chenevier, *Chem. Eur. J.* **2009**, *15*, 2101 – 2110.
[38] J. Ramirez, M. L. Mayo, S. Kilina, S. Tretiak, *Chem. Phys.* **2013**, *413*, 89 – 101.
[39] O. R. Luca, J. L. Gustafson, S. M. Maddox, A. Q. Fenwick, D. C. Smith, *Org. Chem. Front.* **2015**, *2*, 823 – 848.
[40] E. S. Lewis, *J. Am. Chem. Soc.* **1989**, *111*, 7576 – 7578.
[41] M. D. Watson, M. G. Debije, J. M. Warman, K. Müllen, *J. Am. Chem. Soc.* **2004**, *126*, 766 – 771.
[42] Y.-Z. Tan, B. Yang, K. Parvez, A. Narita, S. Osella, D. Beljonne, X. Feng, K. Müllen, *Nat. Commun.* **2013**, *4*, 2646 – 2653.

Manuscript received: June 25, 2017
Accepted manuscript online: August 6, 2017
Version of record online: August 23, 2017

